Contents lists available at ScienceDirect

Optics Communications

journal homepage: www.elsevier.com

# Broadband anti-reflection coating using dielectric $Si_3N_4$ nanostructures. Application to amorphous-Si-H solar cells

M.H. Elshorbagy [a, b], Kamal Abdel-Hady [b], Hala Kamal [a], Javier Alda [a, *]

[a] Applied Optics Complutense Group, University Complutense of Madrid, Faculty of Optics and Optometry, Av. Arcos de Jalon, 118, 28037 Madrid, Spain
[b] Physics Department, Faculty of Science, Minia University, El-Minya, Egypt

ARTICLE INFO

*Keywords:*
Resonant structures
Anti-reflection coating
Light trapping
Solar cell

ABSTRACT

Absorption of amorphous-Si hydrogenated (aSi-H) solar cells can be enhanced by using dielectric nanostructures made of $Si_3N_4$ that work like antireflection coatings. The analysis focus on the short-circuit current delivered by the cell under solar irradiance, and it is made taking into account every layer and structure of an aSi-H cell. A customized design of the antireflection coating in the form of nanostructured dielectric layers, produces a short-circuit current enhancement of 15.2% with respect to the reference flat solar cell, and a lower reflectivity of the cell. Three different geometries of linear nanostructures have been analyzed and compared with quite similar results among them. An improvement in performance has been also obtained for realizable geometrical dimensions that could be fabricated while maintaining electric conductivity of the front contact.

## 1. Introduction

Solar cell technologies are competing among them to improve energy conversion efficiency at cheaper costs [1]. Multi-junction solar cells are obtaining the best figures adjusting their band absorption to the solar spectrum [2]. When restricting the analysis to silicon (Si) based solar cells, we find three major options: single-crystalline Si, multi-crystalline Si, and amorphous Si hydrogenated (aSi-H). From the efficiency point of view, single-crystalline Si is the best option [1], but at higher price and higher manufacture complexity. The low-cost option is represented by aSi-H solar cells. This material has not an indirect band-gap limiting the absorption as in crystalline silicon, and therefore it absorbs better solar radiation. Therefore, around 1 μm layer of aSi-H is thick enough for this application. Actually, its thickness is limited to about 300 nm by material diffusion length. In this case, light trapping mechanisms are important to improve cell performance [3,4]. There exist a strong activity and interest in improving efficiency and related figures of merit. As a consequence, the increase in the short-circuit current, $J_{sc}$, delivered by the structure is one of the goals of several recent proposals and ideas. Even moderate improvements of this parameter are of great interest because they may save materials and space in solar power stations relying on this technology. Actually, relative increases in the order of 8–12% have been considered as promising when applied to different types of solar cells incorporating nanostructures and light trapping schemes [5–7]. Large increases in efficiency and $J_{sc}$ are reserved for innovative materials and disruptive technologies.

One of the problems of aSi-H is its structural instability due to the appearance of dangling hydrogen bonds. This mechanism is called Staebler-Wronski Effect (SWE), and it is responsible for up to 20% loss in efficiency because it limits the voltage that could be obtained for aSi-H devices [8]. Fortunately, SWE is reversible with temperature, and defects generated by light irradiation can be mitigated by thermal annealing. This works positively for aSi-H solar cells [8–10]. Then, by using light trapping and confinement strategies, besides improving efficiency, it is possible to increase absorption, generate heat, raise temperature, and partially repair the SWE damage. Several light trapping schemes have been proposed involving plasmonic gratings [11], antireflection coatings [12], photonic crystals [13], waveguides, and dielectric diffractive structures [14]. Guided light increases optical path within the active layer and absorption grows [15]. $Si_3N_4$ thin film Anti-Reflection Coating (ARC) has been positively proved, with optimum thickness values of 60 nm [16,17]. Dielectric subwavelength nanostructures have also been proposed to enhance efficiency for Si-based solar cells [18–21]. In some cases, the proposed structures have been fabricated and realized in practice. The feasibility of fabrication has been also a main concern when considering different geometries and materials in this contribution,

* Corresponding author.
Email address: javier.alda@ucm.es (J. Alda)

http://dx.doi.org/10.1016/j.optcom.2016.12.062
Received 24 October 2016; Received in revised form 17 November 2016; Accepted 26 December 2016
Available online xxx

because large improvements in the performance of the cell can be obtained if fabrication constrains are not fully considered [22].

This paper analyzes the design of $Si_3N_4$ subwavelength nanostructures that work as an ARC, and also traps light towards the aSi-H active layer. This study is made using Comsol Multiphysics as a computational electromagnetism package. The results are positively tested and compared with previous experimental works and modeled designs. The proposed design increases the short-circuit current obtained previously and takes into account all the elements in the structure, and some thickness constrains about the front contact deposition. By considering the whole multilayer structure of the cell we improve the reliability of the results with respect to the case of considering only absorption at the active intrinsic aSi-H layer [22]. The capability to analyze absorption at every layer makes it possible to quantify the amount of energy that, although is not converted into electric power, can still be useful to heat the device and help to mitigate the SWE. Besides, we analyze the effect of the thickness of the front contact layer. This is of importance when proposing ultra-thin front-contact ITO (indium tin oxide) layers that could compromise its electric conductivity. Along the paper we have paid special attention to both absorption, caused by trapping at the proposed nanostructured front layer, and reflectance of the whole cell, which has been reduced with respect to previous reported results [23]. Section 2 of this paper evaluates the contributions of the individual layers of aSi-H solar cell, including the analysis of an optimized flat ARC that combines ITO and $Si_3N_4$. Section 3 presents the main results of the paper when arranging a $Si_3N_4$ nanostructured ARC layer on top of optimum and realizable ITO layers. The results from the numerical evaluation are compared to the reference solar cell. Finally, Section 4 summarizes the main conclusions of this contribution.

## 2. Amorphous-Si-H solar cells

A full characterization of a solar cell begins with the description of the material and geometric arrangement of its structure (see Fig. 1a). Our starting point is the flat configuration aSi-H thin film solar cell ([24]) with the following layer structure (bottom-to-top): Ag (200 nm)/AZO (100 nm)/n-aSi-H (22.4 nm)/i-aSi-H (350.5 nm)/ p-aSi-H (17.5 nm)/ITO (70 nm). n-aSi-H and p-aSi-H are buffer layers that adjust electric field for photo-generated charge carrier separation. The active layer is the i-aSi-H layer, and AZO means ZnO:Al. The refractive index for the i-aSi-H and ITO are obtained from SOPRA material database [25], the refractive index for Ag and $Si_3N_4$ are obtained from [26], and the refractive index for n, p aSi-H and AZO are obtained from [27,28]. Instead of focusing only on the intrinsic active i-aSi-H layer [22], in this paper we have always considered every layer in the solar cell structure. Actually, the thickness of the i-aSi-H active layer is relevant in the overall performance of the cell [29–31]. Larger thickness means larger absorption within the band gap of the material, specially at longer wavelengths. However, this increase reaches an asymptotic value, meaning that a thicker active layer does not produce a significant larger absorption. Table 1 shows the total absorbed power irradiance as a function of thickness of the i-aSi-H active layer. At the same time, the role of the other auxiliary layers should be considered when evaluating the performance of the whole cell and the absorption at the active layer.

Absorption rate is defined as the ratio of absorbed power to incident power, and can be used to calculate the absorptance in each individual layer of the cell by integrating over the volume of each layer. The spectral absorption rate can be calculated as:

$$A(\omega) = \frac{1}{2}\,\omega\varepsilon''|E(\omega)|^2, \tag{1}$$

where $\omega$ is the angular frequency of the incoming radiation, $\varepsilon''$ is the imaginary part of the dielectric permittivity of the material, and $E(\omega)$ is the electric field. As far as we are interested in optical losses in the i-aSi-H layer for an incoming broad-band radiation, we evaluate the absorbed power as:

$$P^i_{abs} = \int A(\omega)\Phi_{\mathrm{AM1.5}}(\omega)d\omega, \tag{2}$$

where $\Phi_{\mathrm{AM1.5}}(\omega)$ is the solar spectral irradiance as a function of frequency [32]. Although Eqs. (1) and (2) are given in terms of the angular frequency, our results will be expressed using wavelength, $\lambda$. In a solar cell we are primarily interested in knowing the short-circuit current, $J_{sc}$, circulating through the structure for a given solar irradiance. This parameter is the one that we need to optimize in a solar cell structure. Assuming that each absorbed photon will create an electron-hole pair contributing to the short-circuit current, $J_{sc}$ can be given in terms of the wavelength as:

$$J_{sc} = \int \frac{q}{hc}A(\lambda)\lambda\Phi_{AM1.5}(\lambda)d\lambda, \tag{3}$$

where $q$ is the electron charge, $c$ is the speed of light in vacuum, and $h$ is the Plancks constant.

To better understand the role of each layer, we have evaluated the individual spectral absorption of them for the reference solar cell

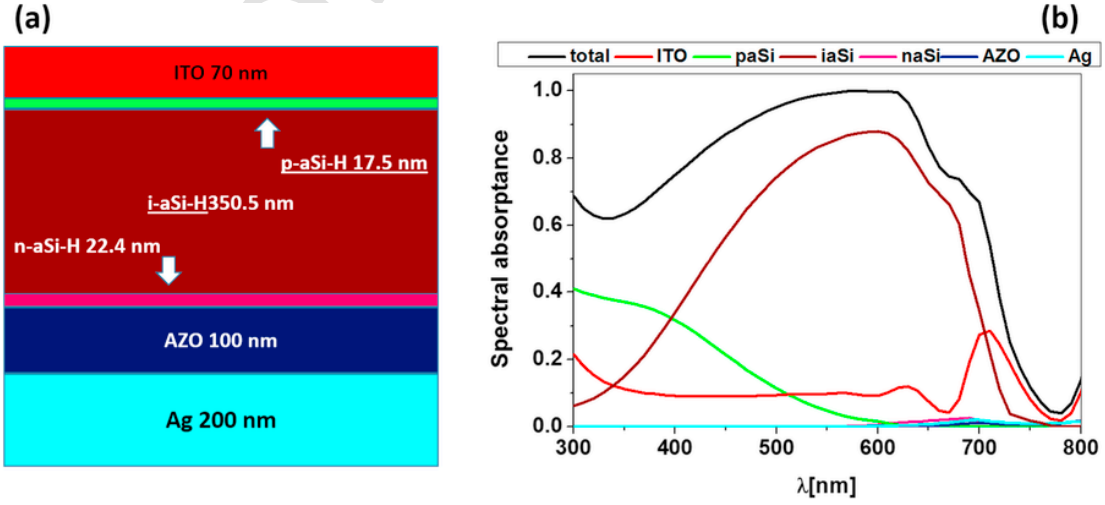


**Fig. 1.** (a) Geometrical arrangement of the layers of a reference solar cell. (b) Spectral absorptance of each layer for the reference cell described in (a).

**Table 1**
Total absorbed power irradiance in i-aSi-H layer for different thicknesses.

| Thickness [nm] | 100 | 200 | 300 | 500 | 1000 |
|---|---|---|---|---|---|
| Absorbed irradiance [W m$^2$] | 183 | 225 | 243 | 251 | 266 |

structure of Fig. 1a. The results are given in Fig. 1b. We may see that, as expected, most of the power is absorbed at the i-aSi-H active layer. However, we can already see how ITO is taking power at longer wavelengths and p-aSi-H buffer layer is also strongly absorbing at shorter wavelengths. The rest of the layers contribute much less to the total absorption, mainly because the amount of optical power reaching layers below the i-aSi-H layer is very little.

An improvement in performance is obtained by using an optimized double-layer antireflection coating made of 10 nm-thick ITO and 60 nm-thick $Si_3N_4$. This geometry enhances optical absorption in both p- and i-aSi-H layers. This ARC also increases the short-circuit current, $J_{sc}$, from 14.35 mA/cm$^2$ for an reference cell (70 nm-thick ITO layer), to 15.54 mA/cm$^2$ for the cell with this optimized double ARC, which is about 8.3% enhancement. In Fig. 2a and b we can see how the improvement appears a every wavelength both for the i-aSi-H layer and the total structure. The main issue with this double-layer ARC is the increase in electric resistivity of a 10 nm-thick ITO layer. This could compromise its capability to work as a front contact. Besides, these structures need complex ultra-thin fabrication techniques [33,34].

## 3. Dielectric nanostructures for aSi-H cells

In the previous section we have evaluated the individual contributions of the layers of a reference aSi-H solar cell. Besides, we have seen how an optimized $Si_3N_4$/ITO ARC improves the performance of solar cells. In this section, we now analyze the use of dielectric nanostructures made of $Si_3N_4$. These nanostructures, when properly arranged and deposited on top of the ITO layer, increase $J_{sc}$. To demonstrate that, we have selected a simple grating geometry (see Fig. 3a), being $H$ the height of the groove, $w$ its width and $s$ its separation (the period of the grating is $p = w + s$). $H$ is fixed at a value of 60 nm. To better compare the results with previous results, we set the thickness of the ITO layer to 10 nm. Besides the rectangular profile of the grating, we have also considered a trapezoidal and triangular shape with parameters *tw* and *bw*. When evaluating the electromagnetic behavior of this structure we find that, at some resonant wavelengths, Poynting vector inside the active layer is enhanced when using the proposed dielectric nanostructures (see Fig. 3b). These resonances also appear as peaks in the spectral absorption (see Fig. 2). The rectangular structure can be fabricated by evaporating $Si_3N_4$, or by etching a 60 nm-thick flat $Si_3N_4$ layer, along the predefined pattern. Trapezoidal profiles could be fabricated with the same nanoimprinting technology applied to Blu-Ray disc manufacture [35].

The optimization of the proposed nanostructured ARC layer is made by maximizing the short-circuit current, $J_{sc}$, when varying $w$ and $s$ for the rectangular shape case. The increase in $J_{sc}$ is due to the trapping of light caused by the nanostructure (see Poynting vector maps in Fig. 3b). Fig. 4a shows as a map, the value of $J_{sc}$ in terms of $w$ and $s$ geometrical parameters, maintaining $H = 60$ nm. We may check that a maximum value of $J_{sc} = 16.54$ mA/cm$^2$ is obtained when $w = 250$ nm and $s = 150$ nm ($p = 400$ nm). This value is 15.2% larger than the reported value of 14.35 mA/cm$^2$ corresponding to the reference aSi-H cell, and even 6.3% larger than the $J_{sc}$ obtained for an optimized double layer ($Si_3N_4$/ITO) ARC. This design will be considered as optimal for rectangular shape nanostructured ARC. From Fig. 4a, we can see that, although we have selected the point where $J_{sc}$ is reaching a maximum value, it is possible to find quite similar values combining geometric parameters properly. This behavior makes it possible to select those parameters taking into account fabrication constrains. The optimization was made using TE polarization. We have checked that TE and TM polarization behave very similarly. As far as the solar cells work with natural light, in the following we will average the results obtained from TE and TM polarization states. By using the transverse parameters that optimize the nano-rectangular structure ($w = 250$ nm, $s = 150$ nm), we have also optimized the other two nanostructures (triangular, and trapezoidal) by varying $H$. The results are presented in Fig. 4b and show that similar values of $J_{sc}$ to those obtained for a nano-rectangular shape, can be achieved when using other geometries. Therefore, more light is arriving to the active i-aSi-H layer when using a nanostructured ARC. This is proved by evaluating absorption only at the i-aSi-H layer spectrally, but having all the layers modeled and considered. In Fig. 2a, we can clearly see how optimized nanostructured devices absorb more than flat solar cells along the whole spectral range. Those absorption peaks appearing at 718 nm and 740 nm correspond to the trapping model shown in Fig. 3b. The total spectral absorption of the reference cell, the flat ARC cell, and the optimum nanostructured ARC cell, are shown in Fig. 2b. It is also interesting to compare the total absorbed power of the reference solar cell (471.2 W/m$^2$), the double-layer flat ARC (426.2 W/m$^2$), and the optimized rectangular nanostructured ARC (474.1 W/m$^2$). We may see that nanostructured ARC recovers the

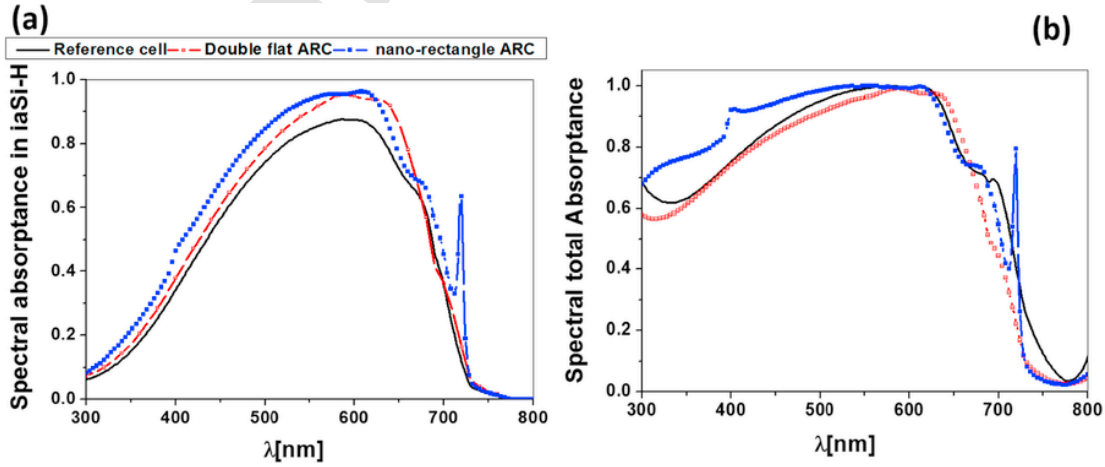


**Fig. 2.** Spectral absorptance at the i-aSi-H layer (a), and total spectral absortion of the whole cell (b) for three cases: Standard aSi-H cell (used as reference), aSi-H cell having a $Si_3N_4$/ITO ARC, and optimized nanostructure with rectangular shape.

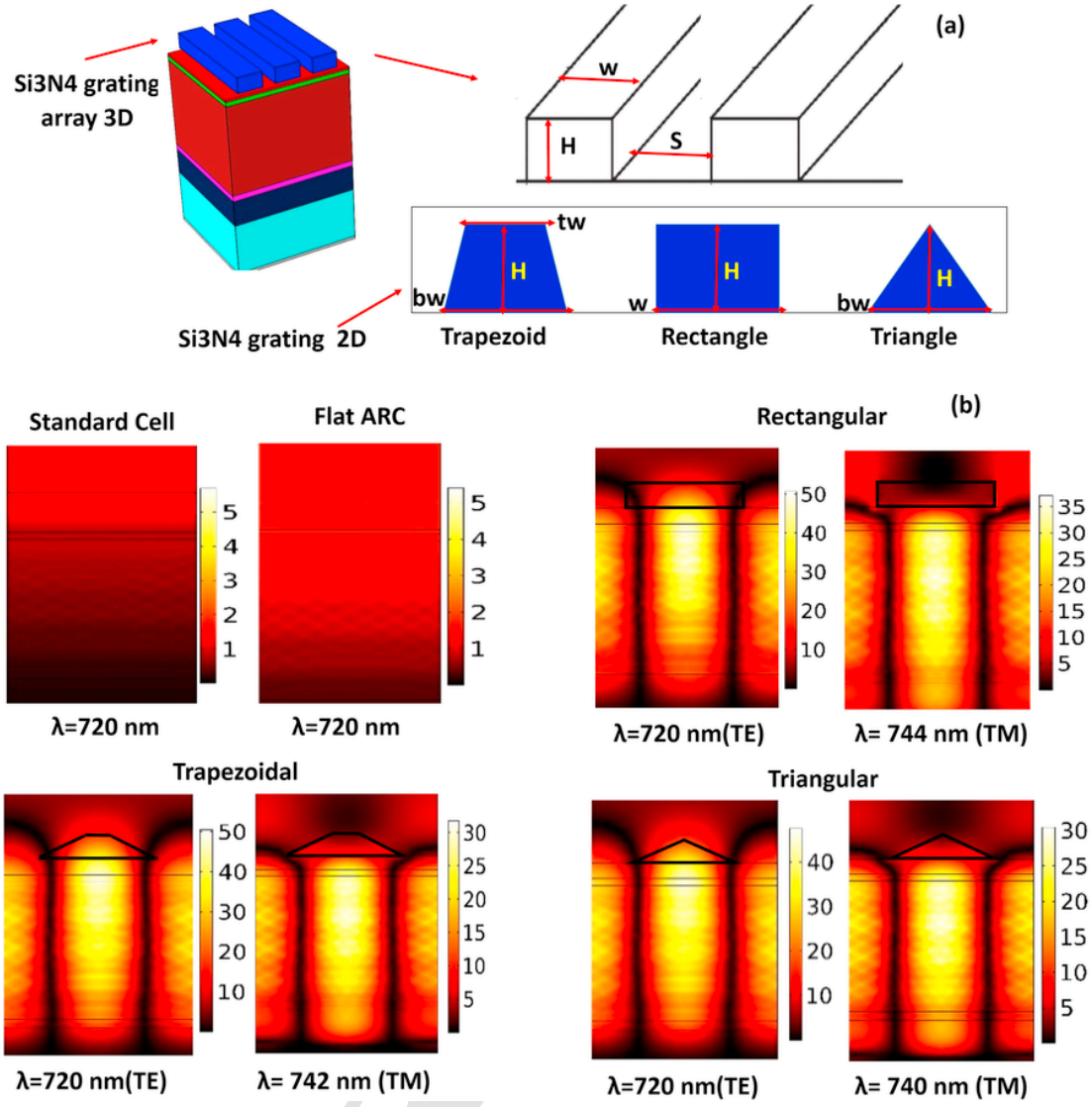


**Fig. 3.** (a) Diagram for the patterned cell showing the profile of the nanostructure and their geometric parameters. (b) Maps of the Poynting vector at two wavelengths for the reference, and optimized flat ARC, and for the three proposed shapes of the nanostructured ARC (triangle, trapezoid, and rectangle). The wavelengths showing this trapping correspond with the absorption peaks shown in Fig. 2.

value of total absorption of the reference cell. At this point we should remember that increasing absorption helps to heat the cell, and this thermal dissipation improves the repairing effect of those damages caused by SWE [8].

### 3.1. Reflectivity

Reflectivity is another important parameter describing how these nanostructures work. Fig. 5 shows reflectivity for the optimum designs analyzed in this paper. Comparing the results for absorption reported in Fig. 2a for the reference cell and the flat double-layer ARC with those given in Fig. 5, we may see that, although absorption at the i-aSi-H layer is enhanced when using ARC, reflectivity is about the same for these two designs. This means that light is better trapped at the i-aSi-H layer when ARC is in place. At the same time, the ITO thickness reduction (from 70 nm to 10 nm) of the double-layer flat ARC contributes to lower absorption within the ITO layer. This also means that when using a nanostructured ARC having an ultra-thin 10 nm-thick ITO layer, reflectivity is significantly lower within a broad-band region (300–500 nm) than for the double-layer flat ARC, and the reference solar cell (see Fig. 5).

As an additional remark to emphasize the goodness of the proposed nanostructures designs, we show in Table 2 the reflectivity values for the optimum designs obtained previously, for two different spectral ranges. The range between 300 nm and 700 nm describes the spectral region where the photovoltaic conversion occurs. The extended range between 300 nm and 900 nm includes the near infrared where absorbed light is better absorbed as heat. Also in this region reflectivity is lower for the nanostructured case meaning larger absorption contributing to repair SWE damage. Previously reported values of reflectance for antireflection coatings in solar cells are around 25% [23]. The total reflectance obtained by the optimized proposed nanostructure is around 20%, improving absorption on the cell structure.

### 3.2. Thickness of the ITO layer

When describing the double-layer flat ARC structure we were concerned about the front contact thickness. These flat ARC struc-

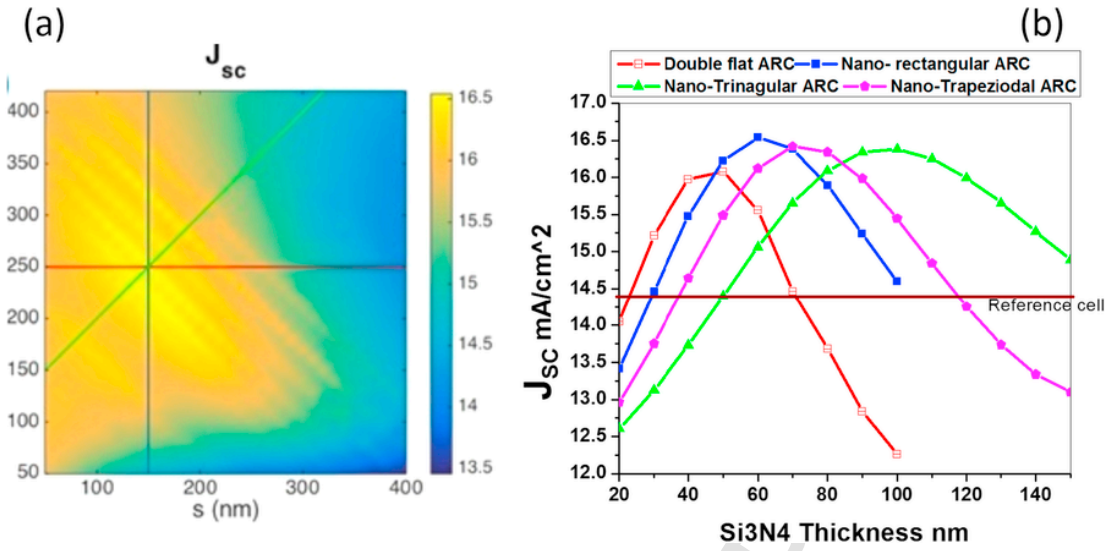


**Fig. 4.** (a) Map of the value of $J_{sc}$ as a function of the geometric parameters $w$ and $s$. (b) Parametric dependence of $J_{sc}$ when varying $H$ for different ARC designs, including the flat ARC with no nanostructures.

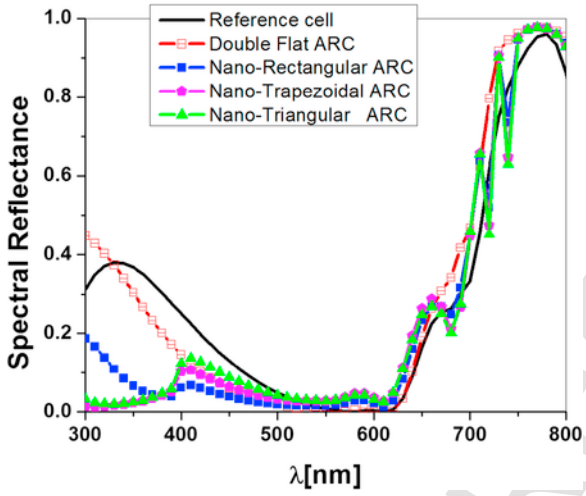


**Fig. 5.** Spectral reflectivity for the optimum designs analyzed in this paper.

**Table 2**
Total reflectivity for the proposed designs in two spectral ranges. The number in parenthesis correspond with the relative change with respect to the standard reference cell.

| Structure | $R_{\text{total}}$ % | $R_{\text{total}}$ % |
|---|---|---|
| | [300–700 nm] | [300–900 nm] |
| Reference cell | 6.40 | 31.24 |
| Flat ARC | 5.66 (−11.56) | 24.02 (−23.11) |
| Nano-rectangular | 3.34 (−47.81) | 20.64 (−33.93) |
| Nano-trapezoidal | 3.24 (−49.38) | 20.34 (−34.89) |
| Nano-triangular | 3.45 (−46.09) | 20.50 (−34.38) |

tures are optimized by using a very thin ITO layer of about 10 nm. For a nanostructured ARC described previously, the dielectric grating is patterned on top of this ITO layer. However, this ultra-thin ITO layer may compromise the electrical performance of the device, and requires special care to homogenize the finishing quality of the ITO layer. A more reliable thickness value, that maintains good optical and electrical properties in reference solar cells, is around 35–40 nm [34]. Using a 40 nm-thick ITO layer, we have performed an optimization and comparison of the three grating geometries presented here: rectangular, trapezoidal, and triangular. The results, in terms of $J_{sc}$, are given in Table 3. In this table we have also reported $J_{sc}$ for a solar cell having a double $Si_3N_4$/ITO ARC with a non-optimal ITO thickness of 40 nm as a double-layer flat ARC with better fabrication parameters. The reference value of 14.35 mA/cm$^2$ for an reference aSi-H cell is surpassed when adding the optimized nanostructure. When analyzing the spectral absorption at the i-aSi-H layer (see Fig. 6a), and reflectivity of the whole structure (see Fig. 6b), we see how reflection is reduced as absorption increases. This means a larger number of generated free carriers that improves current, and a larger absorption within the structure that increases temperature and helps to mitigate SWE damage. In Fig. 6c we have also included a power budget of how absorption is distributed among the layers of the cell for different cases. This graphical representation shows how the thickness of ITO layer strongly changes the portion of energy absorbed at the front contact.

After comparing these designs for a fixed ITO thickness, we have performed an analysis in terms of the ITO thickness for the optimum ARC proposed in this paper, taking $J_{sc}$ as the parameter of interest. Fig. 7a shows the three optimum nanostructure shapes behaving better than double-layer flat ARC for every ITO thickness. At the same time, if we consider the nanostructures having a common value of its thickness, $H=60$ nm, it is still possible to generate a larger current for thickness values around 20–30 nm. Actually, triangular nanostructures on top of a 30 nm-thick ITO layer produces a value of

**Table 3**
Short-circuit current, $J_{sc}$, for the nanostructured design when using a 40 nm-thick ITO layer for all the cases, except for the reference solar cell where the ITO layer is 70 nm thick (Ref).

| Structure | Nano-triangle ARC | Nano-trapezoid ARC | Nano-rectangle ARC | Flat ARC | Ref |
|---|---|---|---|---|---|
| $J_{sc}$ (mA/cm$^2$) | 15.68 | 15.62 | 14.99 | 12.5 | 14.35 |

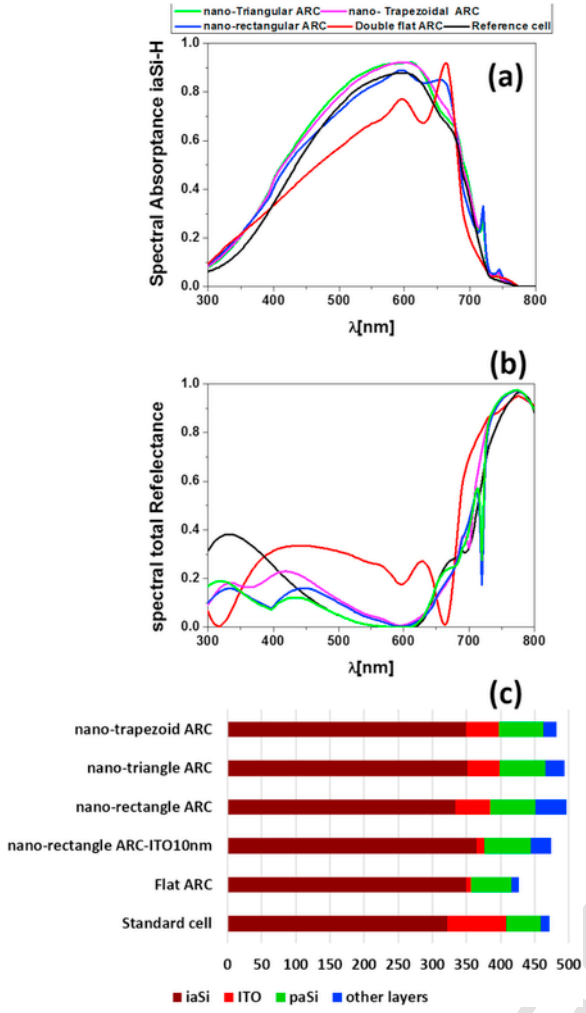


**Fig. 6.** (a) Spectral absorptance at the i-aSi-H layer. (b) Total spectral absorption. (c) Power budget distribution among the layers of the cell for various designs. The black dotted line is for the optimized double layer ARC with 40 nm-thick ITO layer. The black solid line is for the optimized nanostructured ARC with a 40 nm-thick ITO layer.

$J_{sc} = 16$ mA/cm$^2$, very close to the optimized value of 16.54 mA/cm$^2$ when rectangular nanostructures are used, and 11.5% larger than that of the reference cell. This means that, by changing the geometry of the profile we can compensate for the loss in performance due to a thicker ITO layer. Fig. 7 also determines the practical limits for each structure depending on the minimum practical ITO thickness that could achieve the maximum enhancement.

## 4. Conclusions

The fabrication technology and material preparation of aSi-H cells are simpler and comparatively cheaper than high-performance solar cells. Because of that, we have analyzed aSi-H cells to enhance their performance. One of the improvements that have been proposed is the customization of antireflection coatings that use front contact ITO layer and a dielectric material on top of it, as for example $Si_3N_4$. A subwavelength nanostructure written on this dielectric material, in combination with the ITO front contact layer, increases significantly the delivered short-circuit current. To ease fabrication we have restricted the nanostructuring to be along one dimension. Then, the 3D structure can be seen as an extruded 2D profile. The geometry of this dielectric nanostructured layer can be fabricated using various techniques such as nano-imprint lithography, ultraviolet lithography, besides e-beam lithography. When using a rectangular shaped profile, we can obtain the desired structure by etching grooves on a flat $Si_3N_4$ layer.

Our analysis has focused on the maximization of the short-circuit current delivered by the cell. We have taken into account every layer of the cell: top and bottom contacts, n, p, and i-aSi-H layers, and even buffer layers. By doing this, the results are more reliable and flexible to account for variations of the inner structure of the cell. Besides, with this approach we could evaluate the contribution of every single layer of the cell. These auxiliary layers share some of the enhancement of the optimized structure, and commonly they are not fully considered. However, when total absorption is evaluated, every layer contributes to heat dissipation that helps to repair damages caused by SWE. Our results show how dielectric nanostructures can lower reflectivity and increase absorptance within the active i-aSi-H layer, modifying the power budget distribution between layers. An optimum configuration of $Si_3N_4$ subwavelength grating structures increases short-circuit current 15.2% with respect to a reference aSi-H solar cell. Enhancement is still significant when compared with a solar cell having an optimized non-structured double ARC. Although the increase in performance, given by the enhancement of the short-circuit current, $J_{sc}$, could be considered moderate, this value is higher than some other geometries proposed in the literature that range around 8–12%. Besides absorption at the intrinsic layer, we have also evaluated the total reflectance of the cell, obtaining values for this parameter around 20% that is lower than some other optimized antirreflection coatings that account for reflectance values around 25%. Therefore, the proposed structure means better absorption and improved performance.

Some of the proposed designs use ultra-thin ITO layer that need careful fabrication and may compromise the electric behavior of this front contact. This fact has been taken into account in this paper by analyzing the effect of a feasible, although non-optimal, thickness of this layer in conjunction with deposition of a thin $Si_3N_4$ layer. Even in this case, nanostructured ARC improves the value of the short-circuit current around 11.5% for a trapezoidal grating on a 30 nm ITO layer.

Summarizing the findings of this paper, we have seen that by nanostructuring a front dielectric layer on top of t aSi-H solar cells, it is possible to improve significantly the performance of aSi-H solar cells. Besides, we have found how incoming energy is distributed along the structure of the cell, allowing a better knowledge of the contribution of each layer. Computational electromagnetism has been used here to analyze how light is guided into the active layer, revealing spectral resonances due to light interaction with dielectric nanostructures. This contribution shows how it is still possible to improve a well-established design by using auxiliary nanostructures properly optimized.

## Acknowledgement

This work was partially supported by the Egyptian ministry of higher education missions section under Egyptian Co-supervision Grant at UCM Spain. We would like to thank the Egyptian institute, cultural office of the Egyptian embassy in Madrid Spain. This work has been partially supported by project TEC2013-40442 from the Spanish Ministerio of Economía and Competitividad.

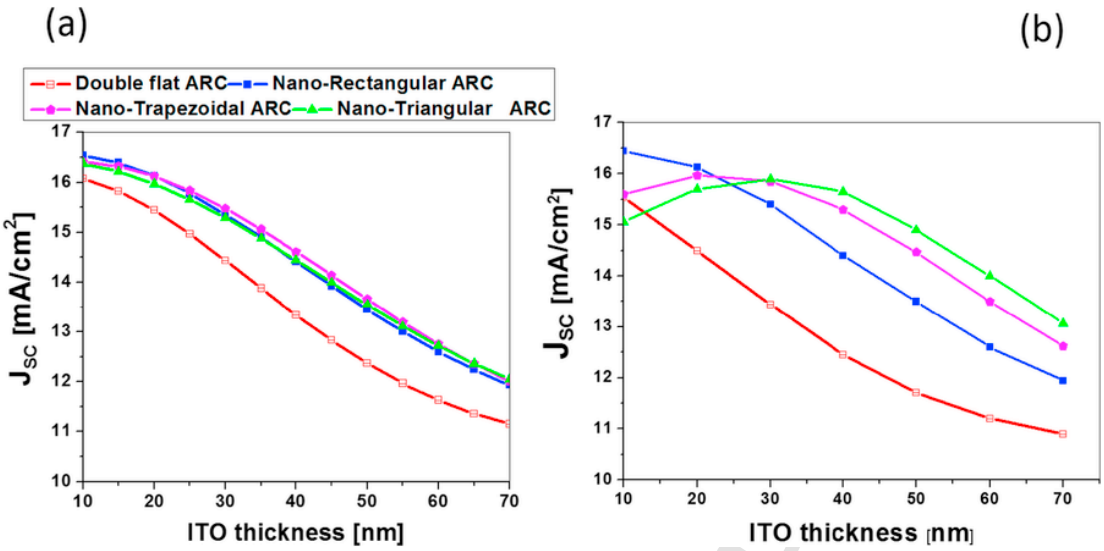


**Fig. 7.** Short-circuit current, $J_{sc}$, for different structures as a function of the ITO thickness. (a) Optimized nanostructures behave better for every value of the ITO thickness. (b) Optimized nanostructures with a fixed value of $H=60$ nm for triangular and trapezoidal geometries. In this case, depending on the profile geometry the system behaves better for a given optimum value of the thickness of the ITO layer.

## References


[1] M.A. Green, K. Emery, Y. Hishikawa, W. Warta, E.D. Dunlop, Solar cell efficiency tables (version 45), Prog. Photovolt.: Res. Appl. 23 (1) (2015) 1–9, http://dx.doi.org/10.1002/pip.2573.

[2] M.K. Siddiki, J. Li, D. Galipeau, Q. Qiao, A review of polymer multijunction solar cells, Energy Environ. Sci. 3 (7) (2010) 867–883, http://dx.doi.org/10.1039/B926255P.

[3] Y. Abdulraheem, I. Gordon, T. Bearda, H. Meddeb, J. Poortmans, Optical bandgap of ultra-thin amorphous silicon films deposited on crystalline silicon by pecvd, AIP Adv. 4 (5) (2014) 057122, http://dx.doi.org/10.1063/1.4879807.

[4] K. Hattori, H. Okamoto, Y. Hamakawa, Theory of the steady-state-photocarrier-grating technique for obtaining accurate diffusion-length measurements in amorphous silicon, Phys. Rev. B 45 (3) (1992) 1126, http://dx.doi.org/10.1103/PhysRevB.45.1126.

[5] W.-C. Hsu, J.K. Tong, M.S. Branham, Y. Huang, S. Yerci, S.V. Boriskina, G. Chen, Mismatched front and back gratings for optimum light trapping in ultra-thin crystalline silicon solar cells, Opt. Commun. 377 (2016) 52–58. (?http://dx.doi.org/10.1016/j.optcom.2016.04.055?URL ?http://www.sciencedirect.com/science/article/pii/S0030401816303303?).

[6] J. Hao, Y. Xu, S. Chen, Y. Zhang, J. Mai, T.-K. Lau, R. Zhang, Y. Mei, L. Wang, X. Lu, W. Huang, Broadband plasmon-enhanced polymer solar cells with power conversion efficiency of 9.26% using mixed au nanoparticles, Opt. Commun. 362 (2016) 50–58. (polymer Photonics and Its Applications. ?http://dx.doi.org/10.1016/j.optcom.2015.07.032?URL ?http://www.sciencedirect.com/science/article/pii/S0030401815006276?).

[7] K. Huang, Q. Wang, X. Yan, K. Hu, M. Yu, X. Shen, Demonstration of enhanced absorption in thin film si solar cells with periodic microhemisphere hole arrays, Opt. Commun. 315 (2014) 79–82. (?http://dx.doi.org/10.1016/j.optcom.2013.10.014?URL ?http://www.sciencedirect.com/science/article/pii/S0030401813009188?).

[8] D. Staebler, C. Wronski, Reversible conductivity changes in discharge-produced amorphous si, Appl. Phys. Lett. 31 (4) (1977) 292–294, http://dx.doi.org/10.1063/1.89674.

[9] E. Radziemska, The effect of temperature on the power drop in crystalline silicon solar cells, Renew. Energy 28 (1) (2003) 1–12, http://dx.doi.org/10.1016/S0960-1481(02)00015-0.

[10] M. Pathak, J.M. Pearce, S. Harrison, Effects on amorphous silicon photovoltaic performance from high-temperature annealing pulses in photovoltaic thermal hybrid devices, Sol. Energy Mater. Sol. Cells 100 (2012) 199–203, http://dx.doi.org/10.1016/j.solmat.2012.01.015.

[11] J.N. Munday, H.A. Atwater, Large integrated absorption enhancement in plasmonic solar cells by combining metallic gratings and antireflection coatings, Nano Lett. 11 (6) (2010) 2195–2201, http://dx.doi.org/10.1021/nl101875t.

[12] J. Zhao, M.A. Green, Optimized antireflection coatings for high-efficiency silicon solar cells, IEEE Trans. Electron Devices 38 (8) (1991) 1925–1934, http://dx.doi.org/10.1109/16.119035.

[13] P. Bermel, C. Luo, L. Zeng, L.C. Kimerling, J.D. Joannopoulos, Improving thin-film crystalline silicon solar cell efficiencies with photonic crystals, Opt. Express 15 (25) (2007) 16986–17000, http://dx.doi.org/10.1364/OE.15.016986.

[14] M. Kroll, S. Fahr, C. Helgert, C. Rockstuhl, F. Lederer, T. Pertsch, Employing dielectric diffractive structures in solar cells-a numerical study, Physica Status Solidi (a) 205 (12) (2008) 2777–2795, http://dx.doi.org/10.1002/pssa.200880453.

[15] P.N. Saeta, V.E. Ferry, D. Pacifici, J.N. Munday, H.A. Atwater, How much can guided modes enhance absorption in thin solar cells?, Opt. Express 17 (23) (2009) 20975–20990, http://dx.doi.org/10.1364/OE.17.020975.

[16] K. Islam, A. Alnuaimi, H. Ally, A. Nayfeh, Ito, si3n4 and zno: Al–simulation of different anti-reflection coatings (arc) for thin film a-si: H solar cells, in: Proceedings of the IEEE on Modelling Symposium (EMS), European, 2013, pp. 673–676 http://dx.doi.org/10.1109/EMS.2013.112.

[17] I. Massiot, C. Colin, N. Péré-Laperne, P.R.i. Cabarrocas, C. Sauvan, P. Lalanne, J.-L. Pelouard, S. Collin, Nanopatterned front contact for broadband absorption in ultra-thin amorphous silicon solar cells, Appl. Phys. Lett. 101 (16) (2012) 163901, http://dx.doi.org/10.1063/1.4758468.

[18] K.C. Sahoo, E.Y. Chang, Y. Li, M.-K. Lin, J.-H. Huang, Fabrication and configuration development of silicon nitride sub-wavelength structures for solar cell application, J. Nanosci. Nanotechnol. 10 (9) (2010) 5692–5699, http://dx.doi.org/10.1166/jnn.2010.2553.

[19] J. Buencuerpo, J. Llorens, M. Dotor, J. Ripalda, Broadband antireflective nano-cones for tandem solar cells, Opt. Express 23 (7) (2015) A322–A336, http://dx.doi.org/10.1364/OE.23.00A322.

[20] K.C. Sahoo, M.-K. Lin, E.-Y. Chang, T.B. Tinh, Y. Li, J.-H. Huang, Silicon nitride nanopillars and nanocones formed by nickel nanoclusters and inductively coupled plasma etching for solar cell application, Jpn. J. Appl. Phys. 48 (12R) (2009) 126508, http://dx.doi.org/10.1143/JJAP.48.126508.

[21] Y. Li, M.-Y. Lee, H.-W. Cheng, Z.-L. Lu, 3d simulation of morphological effect on reflectance of si3n4 sub-wavelength structures for silicon solar cells, Nanoscale Res. Lett. 7 (1) (2012) 1–6, http://dx.doi.org/10.1186/1556-276X-7-196.

[22] S. Saravanan, R. Dubey, Optical absorption enhancement in 40 nm ultrathin film silicon solar cells assisted by photonic and plasmonic modes, Opt. Commun. 377 (2016) 65–69. (?http://dx.doi.org/10.1016/j.optcom.2016.05.028?URL ?http://www.sciencedirect.com/science/article/pii/S0030401816303807?).

[23] A.J. Haider, A.A. Najim, M.A. Muhi, Tio2/ni composite as antireflection coating for solar cell application, Opt. Commun. 370 (2016) 263–266http://dx.doi.org/10.1016/j.optcom.2016.03.034. http://www.sciencedirect.com/science/article/pii/S0030401816301985..

[24] A. Vora, J. Gwamuri, J.M. Pearce, P.L. Bergstrom, D.Ö. Güney, Multi-resonant silver nano-disk patterned thin film hydrogenated amorphous silicon solar cells for staebler-wronski effect compensation, J. Appl. Phys. 116 (9) (2014) 093103, http://dx.doi.org/10.1063/1.4895099.

[25] SOPRA, Refractive Index Librarary, URL ?http://www.sspectra.com/sopra.html?.

[26] Refractive info database, Refractive Index Librarary, URL ?http://refractiveindex.info?.

[27] Z.C. Holman, A. Descoeudres, L. Barraud, F.Z. Fernandez, J.P. Seif, S. De Wolf, C. Ballif, Current losses at the front of silicon heterojunction solar cells, IEEE J. 2 Photovolt. 1 (2012) 7–15. (?http://dx.doi.org/Currentlossesatthefrontofsiliconheterojunctionsolarcells?).

[28] R. Treharne A. Seymour-Pierce K. Durose K. Hutchings S. Roncallo D. Lane Optical design and fabrication of fully sputtered cdte/cds solar cells J. Phys.: Conf. Ser. 286 (2011) 012038 http://dx.doi.org/10.1088/1742-6596/286/1/012038

[29] A. Belfar, The role of p+-layer dopant concentration, p+-layer band gap and p+-layer thickness in the performances of a-si: H n-i-p-p+ solar cells with double layer window nanocrystalline silicon, Opt.-Int. J. Light Electron

Opt. 126 (24) (2015) 5688–5693, http://dx.doi.org/10.1016/j.ijleo.2015.09.026.
[30] S. Singh, S. Kumar, N. Dwivedi, Band gap optimization of p-i-n layers of a-si: H by computer aided simulation for development of efficient solar cell, Sol. Energy 86 (5) (2012) 1470–1476, http://dx.doi.org/10.1016/j.solener.2012.02.007.
[31] M. Sharma, S. Juneja, S. Sudhakar, D. Chaudhary, S. Kumar, Optimization of a-si: H absorber layer grown under a low pressure regime by plasma-enhanced chemical vapor deposition: revisiting the significance of the p/i interface for solar cells, Mater. Sci. Semicond. Process. 43 (2016) 41–46, http://dx.doi.org/10.1016/j.mssp.2015.10.021.
[32] NERL, Spectral Solar Irriadiance, URL ?http://rredc.nrel.gov/solar/spectra/am1.5/?.
[33] E.-J. Guo, H. Guo, H. Lu, K. Jin, M. He, G. Yang, Structure and characteristics of ultrathin indium tin oxide films, Appl. Phys. Lett. 98 (1) (2011) 011905, http://dx.doi.org/10.1063/1.3536531.
[34] J. Gwamuri, A. Vora, J. Mayandi, D.Ö. Güney, P.L. Bergstrom, J.M. Pearce, A new method of preparing highly conductive ultra-thin indium tin oxide for plasmonic-enhanced thin film solar photovoltaic devices, Sol. Energy Mater. Sol. Cells 149 (2016) 250–257, http://dx.doi.org/10.1016/j.solmat.2016.01.028.
[35] B.-R.D. Association, Blu-ray disc format, White paper, 3rd. edition, Blu-Ray Disc Association, 2012.